Biochemical Characterization of RAR1 Cysteine- and Histidine-Rich Domains (CHORDs): A Novel Class of Zinc-Dependent Protein−Protein Interaction Modules†

Charles T. Heise,‡ Cécile S. Le Duff,§ Marta Boter,|| Catarina Casais,|| Joanne E. Airey,‡ Andrew P. Leech,‡ Béatrice Amigues,⊥ Raphaël Guerois,⊥ Geoffrey R. Moore,§ Ken Shirasu,||,# and Colin Kleanthous*,‡

Department of Biology, University of York, Post Office Box 373, York, YO10 5YW, United Kingdom, School of Chemical Sciences and Pharmacy, University of East Anglia, Norwich, NR4 7TJ, United Kingdom, The Sainsbury Laboratory, The John Innes Centre, Colney Lane, Norwich, NR4 7UH, United Kingdom, and Service de Biophysique des Fonctions Membranaires, CEA/Saclay, F-91191 Gif-sur-Yvette, France

Received October 19, 2006; Revised Manuscript Received November 24, 2006

ABSTRACT: Disease resistance in plants requires the activation of defense signaling pathways to prevent the spread of infection. The protein Required for Mla12 Resistance (RAR1) is a component of such pathways, which contains cysteine- and histidine-rich domains (CHORDs) that bind zinc. CHORDs are 60 amino acid domains, usually arranged in tandem, found in almost all eukaryotes, where they are involved in processes ranging from pressure sensing in the heart to maintenance of diploidy in fungi, and exhibit distinct protein−protein interaction specificity. In the case of RAR1, CHORD-I is known to interact with heat-shock protein 90 (HSP90) and CHORD-II is known to interact with the Suppressor of the G2 allele of Skp1 (SGT1). The focus of this work on RAR1 from barley and *Arabidopsis* was to address the paucity of biochemical information on RAR1 and its constituent CHORDs, particularly the role of the metal ion. Sedimentation experiments indicated RAR1 to be an extended monomer in solution with few intramolecular interactions. This was reinforced by denaturation experiments, where little difference between the stability of the individual domains and intact RAR1 could be detected by intrinsic tryptophan fluorescence. Electrospray ionization−mass spectrometry and atomic absorption showed that, contrary to previous reports, RAR1 binds five zinc ions; each CHORD binds two, and the plant-specific, 20 amino acid cysteine- and histidine-containing motif (CCCH motif) located between the two CHORDs binds the fifth. Fluorescence, ultraviolet circular dichroism (UV CD), and nuclear magnetic resonance (NMR) spectroscopy further demonstrated that zinc ions are essential for maintaining CHORD structure. Finally, we used isothermal titratrion colarimetry to show that zinc is essential for the specific binding interactions of CHORD-II with SGT1. Our study provides the first biochemical and biophysical data on the zinc metalloprotein RAR1, defines its metal stoichiometry and that of its constituent CHORDs, and reveals that the metal ions are essential for structural integrity and specific protein−protein associations.

Plants are susceptible to pathogen attack and respond by activating localized cell death through the accumulation of reactive oxygen species to prevent pathogen spread, known as the hypersensitivity response (*1*, *2*). Investigations into the molecular mechanisms of disease resistance have identified the protein Required for Mla12 Resistance (RAR1)[1] as a common component in the signaling pathways triggered by many resistance (R) proteins (*3*−*7*). Initial characterization of RAR1 showed it to be a 25 kDa protein containing two homologous 60 amino acid cysteine- and histidine-rich domains (CHORDs) (*4*), the structure of which remain unknown. CHORD-containing proteins have been found in all eukaryotic genomes, with the exception of yeast, and are usually found in tandem. Sequence alignments of CHORD-containing proteins show two distinct subclasses, the N-terminal CHORD-I and the C-terminal CHORD-II, intimating that each subclass of CHORD carries out a different function (*4*). Each CHORD contains six cysteine and two histidine residues, all of which are conserved and are arranged as two motifs that resemble Cys_3His metal-binding sites (Figure 1). This domain contains two adjacent cysteine residues in the amino acid sequence, which may coordinate zinc as previously seen in the zinc-binding domain from Bruton's tyrosine kinase (*8*). Initial metal analysis, however, indicated that RAR1 bound only two zinc ions, one in each CHORD (*4*).

† This work was funded by the Biotechnology and Biological Sciences Research Council of the U.K.

* To whom correspondence should be addressed. E-mail: ck11@york.ac.uk.
‡ University of York.
§ University of East Anglia.
|| The John Innes Centre.
⊥ Service de Biophysique des Fonctions Membranaires.
Current address: RIKEN Plant Science Center, 1-7-22 Suehiro, Tsurumi, Yokohama 230-0045, Japan.

[1] Abbreviations: RAR1, required for Mla12 resistance; CHORD, cysteine- and histidine-rich domain; CCCH motif, cysteine- and histidine-containing motif; HSP90, heat-shock protein 90; SGT1, suppressor of the G2 allele of skp1; GST, glutathione-*S*-transferase; UV CD, ultraviolet circular dichroism; ESI−MS, electrospray ionization−mass spectrometry; NMR, nuclear magnetic resonance; HSQC, heteronuclear single-quantum coherence; TCEP, tris(2-carboxyethyl) phosphine.

10.1021/bi062174k CCC: $37.00
Published on Web 01/10/2007

A

B

```
                                        CHORD-I
Hv RAR1         CQRIGCDAMF TDDDNPDGSC HYHPSGPLFH DGMKEWSCCK QRSHDFSLFL AIPGCAT-GKH
At RAR1         CQRIGCNAMF TDDDNPQGSC QFHASGPFFH DGMKEWSCCK QRSHDFSLFL EIPGCKT-GKH
Nb RAR1         CQRIGCNATF TEDDNPENSC TYHESGPLFH DGMKKWSCCK KSSHDFSLFL EIPGCKI-GKH
Tg RAR1         CTRPGCGKSY KETENEEGSC VYHAAMPIFH DGVKRWPCCD AEAWDWTDFM AIKGCSF-GKH
Ce CHP-1        CYHKGCGLLF DPKENDNEAC TYHPGGPYFH DAYKIWTCCD KKSTDFGTWM NYKGCTR-GKH
Mm CHP-1        CYNRGCGQRF DPEANSDDAC TYHPGVPVFH DALKGWSCCK RRTTDFSDFL SIVGCTK-GRH
Hs Melusin      CRNKGCGQHF DPNTNLPDSC CHHPGVPIFH DALKGWSCCR KRTVDFSEFL NIKGCTM-GPH
Mm Melusin      CYNKGCGQHF DPNTNLPDSC RYHPGVPIFH DALKGWSCCR KRTVDFSEFL NIKGCTV-GLH
Dm CHP-1        CYNRGCGQLF DPQTNNDESC RHHPGEPFFH DAYKGWSCCN KKSVDFTEFL NIKGCTL-AKH
An CHP-A        CVHKGCGKVF TD---PEEPC VYHPGPPVFH EG-QGWNCCK PRVLTFEEFM EIPPCTT-GKH

                                        CHORD-II
Hv RAR1         CKNKGCGKTY KEKDNHDAAC DYHPGPAVFH DRNRGWKCCD VHVKEFDEFM EIPPCTK-GWH
At RAR1         CKNKGCGQTF KERDNHETAC SHHPGPAVFH DRLRGWKCCD VHVKEFDEFM EIPPCTK-GWH
Nb RAR1         CKNKGCGKTF TEKENHDTAC SYHPGPAIFH DRMRGWKCCD IHVKEFDEFM SISPCTT-GWH
Tg RAR1         CSNKGCNKEY SPNDNSPTAC KFHPGQPVFR DCMKSWTCCQ AKSYDWDEFM KIEPCQT-GPH
Ce CHP-1        CRNNGCSTEF DGSKNKE-NC QHHPGAAIFH EGMKYWSCCN KKTSNFGAFL EQVGCTS-GEH
Mm CHP-1        CKNGGCSKTY QGLQSLEEVC VYHSGVPIFH EGMKYWSCCR RKTSDFNTFL AQEGCTR-GKH
Hs Melusin      CQNPGCDAVY QGPESDATPC TYHPGAPRFH EGMKSWSCCG IQTLDFGAFL AQPGCRV-GRH
Mm Melusin      CQNPGCDAVY QGPESDATPC TYHPGAPRFH EGMKSWSCCG IQTLDFGAFL AQPGCRV-GRH
Dm CHP-1        CKNNGCTYSF TGNSSDFGEC TYHPGVPIFH EGMKFWSCCQ KRTSDFSQFM AQKGCTY-GEH
An CHP-A        CRRRGCGGTYKPDVSRDEERC VYHPGQPVFH EGSKGWSCCK RRVLEFDEFL KIEGCAEKKRH

Concensus       C...GC...# .........C .#H....#FH -.#+.W.CC. ....-#..## ....C...G.H
```

C

```
                    CCCH MOTIF
Hv RAR1         CSRCRQGFFC SDHGSQPKAQ
At RAR1         CSRCRQGFFC SDHGSQPKEQ
Nb RAR1         CPRCRQGFFC SDHGSQPREV
```

FIGURE 1: Domain architecture and sequence aligments of CHORDs from RAR1 homologues. (A) Cartoon of the domain architecture of RAR1, showing CHORDs flanking the plant-specific CCCH motif. The length of the linker regions is shown over the line. (B) Sequence alignments of CHORD-I and CHORD-II with consensus sequence. Conserved residues are shown by a single letter code; putative zinc-binding residues are italicized; #, aromatic; −, negative residues; and +, positive residues. Hv, barley; At, *Arabidopsis*; Nb, tobacco; Tg, toxoplasma; Ce, *C. elegans*; Mm, mouse; Hs, human; Dm, fruit fly; An, *Asperillus*. (C) Sequence alignments of the plant-specific CCCH motif.

The CHORDs of RAR1 are separated by approximately 60 amino acids, which, in plants, contains a conserved 20 amino acid motif designated as the cysteine- and histidine-containing motif (CCCH motif), whose function is unknown (*4*). The diverse distribution of CHORD-containing proteins in biological systems suggests the domains have important functional roles: RAR1 is involved in plant disease resistance; melusin is a pressure sensor in murine cardiac tissue (*9*); CHP-A maintains diploidy in *Aspergillus nidulans* (*10*); and in *Caenorhabditis elegans*, CHP controls germline developmental and embryogenesis (*4*). In addition, mammalian Chp-1, also a RAR1 homologue, was recently identified as a target for transcriptional activation by heat-shock factor 1 (HSF1) (*11*).

Consistent with the distinct sequence conservation of individual CHORDs in eukaryotes, yeast two-hybrid screening and immunoprecipitation assays have shown that the CHORDs of RAR1 interact with different binding partners; CHORD-I binds the chaperone heat-shock protein 90 (HSP90) (*5*, *12*), whereas CHORD-II binds the Suppressor of the G_2 allele of Skp1 (SGT1) (*13*). HSP90 is a highly abundant molecular chaperone, whose role is to stabilize proteins, such as the pre-activated oestrogen receptor or inherently unstable proteins (*14*−*16*). HSP90 is a weak ATPase homodimer, which requires the association of cochaperones to load, stabilize, and release its client proteins (*17*−*20*). SGT1 is also a highly conserved protein, originally identified as an important cell-cycle and kinetochore assembly regulator in yeast (*21*). In plants, it is essential for mediating the release of reactive oxygen species in disease resistance as well as binding the ubiquitinylation machinery of the cell (*22*−*24*). SGT1 has a N-terminal tetratricopeptide repeat (TPR)

domain, a central CHORD−SGT1 motif (CS), which binds CHORD-II, and a C-terminal SGT1-specific (SGS) motif (*4*, *13*, *21*). The CS domain of SGT1 has a similar structure to the HSP90 cochaperone p23 and, similar to p23, is able to bind HSP90 (*5*, *25*−*27*). The TPR domain, usually associated with HSP90 binding, binds poorly or not at all (*5*, *26*, *28*, *29*), and the SGS domain has been shown to interact with leucine-rich repeat (LRR) domains (*30*), as found in several R proteins (*31*, *32*).

The role of RAR1 in resistance signaling appears to be that of interacting with both the protein-folding and degradation machinery. Genetic screens of *RAR1* and *SGT1* mutants in pathogen-challenged plants has led to the suggestion that *in planta* they may be antagonists, with RAR1 acting as a cochaperone stabilizing, HSP90-bound, pre-activated resistance protein, rather than having a direct role in the signal transduction pathway (*33*). SGT1 has been proposed to promote the degradation of R proteins (*13*, *33*), but more recently, it has been suggested that SGT1 functions as a R protein stabilizer (*34*). Interestingly, mouse Chp-1 interacts with HSP90 during the formation of a NOD1−HSP90 complex (*11*). NOD1, a mammalian innate immune receptor, is structurally similar to plant R proteins and also requires HSP90 activity for its stabilization, suggesting a common role for the RAR1 and Chp-1 homologues in disease resistance in plants and mammals (*11*).

Despite extensive work on the *in vivo* functional interactions of RAR1, there is no biochemical or biophysical data on the protein or indeed on any other CHORD-containing protein. Because there are currently no straightforward *in vitro* assays for RAR1 function, we have taken the route of comparing the biophysical and biochemical properties of RAR1 homologues from barley (*Hordeum vulgare*) and *Arabidopsis thaliana*, which share 67% sequence identity (*13*). This has allowed us to determine the characteristic features of RAR1, its individual CHORDs, and their binding interactions.

EXPERIMENTAL PROCEDURES

Gene Constructs. To avoid potential confusion, the *Arabidopsis* gene nomenclature is used in this work regardless of the origin of genes. *A. thaliana* and barley *RAR1* have previously been isolated (*4*, *13*). Three DNA fragments encoding AtRAR1 (full-length *Arabidopsis* RAR1, amino acids 1−226), AtCHORD-I-CCCH (amino acids 1−154), and AtCHORD-II (amino acids 155−226) were cloned into pGEX-6P-1 (Amersham Biosciences, U.K.) using *Eco*RI/*Xho*I to give a glutathione-*S*-transferase (GST) tag and PreScission protease cleavage site N-terminal to the protein. Full-length barley *RAR1* (encoding HvRAR1, amino acids 7−232) and *HvCHORD-I* (amino acids 7−86) were cloned into the pET15b vector (Novagen, U.K.) using *Bam*HI/*Nde*I for *HvRAR1* and *Nde*I/*Hin*dIII for *HvCHORD-I* to give a hexa-His tag and Tobacco Etch Virus (TEV) protease cleavage site (*35*) N-terminal to the protein. The DNA fragment of barley CHORD-II (HvCHORD-II, amino acids 149−232) was cloned into the pETM-30 vector (EMBL, Heidelberg, Germany) using *Nco*I/*Kpn*I to give a N-terminal hexa-His tag, GST tag, and TEV protease cleavage site. Barley *SGT1* (*HvSGT1*) was also cloned into the pET15b vector using *Bam*HI/*Nde*I, placing a hexa-His tag and TEV protease cleavage site N-terminal to the protein. Wheat *HSP90* (*TaHSP90*) was cloned into the pET15b vector using *Bam*HI/*Nde*I to add a N-terminal TEV cleavable His tag for purification. A S-tag::thrombin::HvCHORDI::His-tag construct was used to produce the proteins for nuclear magnetic resonance (NMR) experiments. The protein was cleaved with thrombin, giving a 123-residue protein comprising 107 residues of the HvRAR1 sequence.

Protein Purification. All GST-*Arabidopsis* constructs, His-GST-HvCHORD-II and His-HvSGT1 constructs were overexpressed in *Escherichia coli* BL21 DE3, while His-HvRAR1 and His-HvCHORD-I were expressed in *E. coli* BL21 DE3 containing pLysS and pSBET plasmids (*4*). Bacteria were grown on LB media at 37 °C for all constructs, except His-GST-HvCHORD-II, which was grown at 30 °C. Bacteria were induced with 1 mM final isopropyl-β-D-thiogalactopyranoside (IPTG) (Melford Labs, U.K.) at mid-log phase, and media were supplemented with 50 μM $ZnCl_2$ at the same time. Cells were harvested by centrifugation after 2 h of induction.

His-HvRAR1, His-GST-CHORD-II, and His-HvSGT1 expressing cells were resuspended in 30 mL of buffer A (50 mM Tris-HCl, 150 mM NaCl, 5 mM imidazole, and 50 μM $ZnCl_2$ at pH 7.5) with 1 mM PMSF (Sigma, U.K.) and frozen at −80 °C. Bacteria expressing all of the other GST-fused proteins were resuspended in 30 mL buffer B (10 mM Na_2HPO_4, 2.7 mM KCl, 1.8 mM KH_2PO_4, 150 mM NaCl, and 5 mM dithiothreitol (DTT) at pH 7.3) and stored at −80 °C. Frozen pellets were defrosted and sonicated intermittently for 6 min in a Sonicator 3000 (Misonix, Farmingdale, NY) on an ice slurry and clarified in a Beckman JA25.50 centrifuge rotor (Beckman, Fullerton, CA) at 20 000 rpm for 30 min at 4 °C.

Table 1: Zinc Stoichiometry by Native ESI−MS and Atomic Absorption Spectroscopy[a]

	observed apoprotein mass (Da)	observed native mass (Da)	number of Zn^{2+} (expected native mass)	atomic absorption spectroscopy (zinc/protein ratio)
HvRAR1	24 597.7 ± 1.1	24 914.4 ± 0.7	5 (24 914.7)	4.16 ± 0.06
HvCHORD-I	8635.6 ± 0.6	8762.8	2 (8762.8)	nd
HvCHORD-II	9784.3 ± 1.1	9912.2	2 (9911.8)	nd
AtRAR1	25 745.6 ± 1.3	26 062.3 ± 1.2	5 (26 062.6)	4.61 ± 0.05
AtCHORDI-CCCH	17 490.1 ± 0.7	17 681.2 ± 0.5	3 (17 680.3)	2.67 ± 0.27
AtCHORD-II	9713.4 ± 0.3	9840.6 ± 0.1	2 (9840.2)	1.57 ± 0.43

[a] RAR1 and domain constructs were analyzed for bound metal by ESI−MS in 25 mM ammonium acetate at pH 6.5 as described in the Experimental Procedures. The expected average mass of calculated metal-bound protein [apoprotein + $n$$Zn^{2+}$ − $n$$2H^+$, where Zn = 65.4 (*46*)]. Native ESI−MS of metal-depleted proteins by EDTA gave identical masses for apoproteins to those obtained under denaturing conditions (0.1% formic acid), confirming that all metal had been removed. The protein concentration data for atomic absorption spectroscopy were obtained by the colorimetric assay. All experiments were carried out at least 3 times.

For purification of the His-tagged proteins, the cell extract was loaded onto a 5 mL nitrilotriacetic acid (NTA)-affinity column (Novagen, Madison, WI), precharged with 5 column volumes (CV) of 50 mM $ZnCl_2$, and pre-equilibrated with 5 CV of buffer A. The column was then washed with 5 CV of buffer A, and the protein was eluted with 10 mL of 50 mM Tris-HCl at pH 7.5, 150 mM NaCl, and 750 mM imidazole. DTT was added to a final concentration of 1 mM after elution from the zinc column, and 500 units of TEV protease was added for incubation at 30 °C overnight while dialyzed into buffer C (50 mM Tris-HCl, 150 mM NaCl, 5 mM DTT, and 50 μM $ZnCl_2$ at pH 7.5).

For the purification of the GST-tagged proteins, the clarified supernatant was mixed overnight at 4 °C with 5 mL of 50% slurry of Hi-trap GST Sepharose 4B affinity beads (Amersham Biosciences, U.K.), prewashed in buffer B. Beads were collected by centrifugation (5000 rpm, Sigma 19777 rotor) at 4 °C for 5 min and washed with 20 mL of cold buffer C. The tagged protein was eluted from the beads with 10 mL of cold buffer C containing 10 mM glutathione (Sigma, U.K.). For AtRAR1, AtCHORD-I-CCCH, and AtCHORD-II, the GST tag was removed by the addition of 50 units of PreScisson protease, while the protein was dialyzed against fresh buffer C overnight at 4 °C. For His-GST-HvCHORD-II, the GST tag was removed by the addition of 500 units of TEV protease and dialyzed against fresh buffer C overnight at 30 °C.

After the removal of the purification tag, proteins were gel-filtered on a Superdex 200 gel-filtration column (Amersham Pharmacia, U.K.), equilibrated in buffer C. The eluted protein was then dialyzed into buffer D (20 mM Tris-HCl at pH 7.5, 5 mM DTT, and 50 μM $ZnCl_2$) at 4 °C overnight and subsequently loaded onto a MonoQ 5/5HR column (Amersham Pharmacia, U.K.). The protein was eluted in buffer D with a 0.05−0.15 M NaCl gradient. Clean fractions as determined on reducing 16% sodium dodecyl sulfate−polyacrylamide gel electrophoresis (SDS−PAGE) gel (*36*) were pooled and dialyzed into appropriate buffers for use. RAR1 and CHORDs yielded 1−2 mg L^{-1} pure protein, whereas SGT1 gave >15 mg L^{-1} pure protein. Purified proteins were kept at pH 7.5, unless stated otherwise, because they were found to be pH-sensitive, causing aggregation at high pH or unfolding at low pH.

The S-tag::thrombin::HvCHORD-I::His-tag construct was overexpressed using *E. coli* cells containing pLysS and pSBET on M9 media supplemented with ^{15}N-labeled NH_4Cl and glucose. Bacteria were grown at 30 °C and induced at mid-log phase with a solution of IPTG (final concentration of 1 mM). To test whether Zn^{2+} ions were required for the folding of HvCHORD-I, some flasks were supplemented, while others were not. The protein was purified as described above, and the S tag was cleaved using thrombin overnight at 4 °C in thrombin cleavage buffer. The HvCHORD-I::His-tag construct was subsequently cleaned using gel-filtration chromatography on a Superdex 75 column equilibrated in 20 mM Tris at pH 7.5, 400 mM NaCl, and 5 mM DTT.

Protein Concentration Determination. The protein concentration was generally determined by the Bradford assay (BioRad, U.K.). Protein concentrations were also measured by absorbance at 280 nm using calculated extinction coefficients: AtRAR1, 16 500 $(M\ cm)^{-1}$; AtCHORD-II, 11 000 $(M\ cm)^{-1}$; and HvSGT1, 43 240 $(M\ cm)^{-1}$ (us.expasy.org).

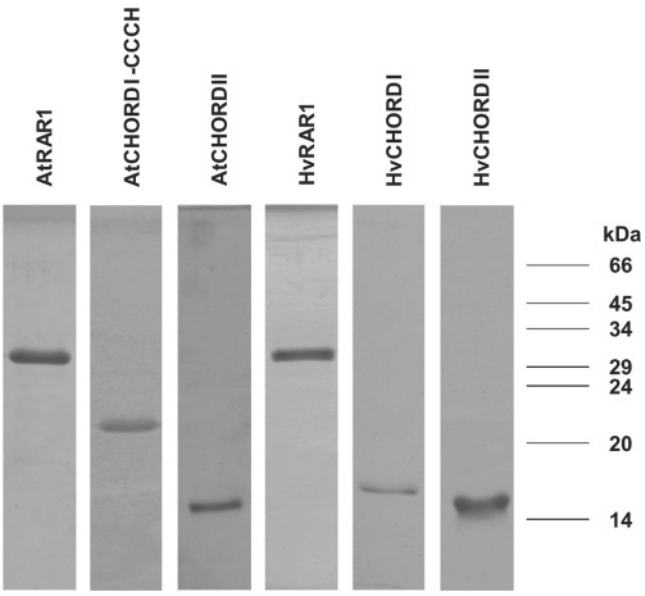

FIGURE 2: Purity of expressed RAR1 and CHORD constructs. Coomassie-stained SDS−PAGE gels (16%, reducing) of purified *E. coli* expressed RAR1 constructs from barley (Hv) and *Arabidopsis* (At) after Mono Q column. The identity of purified proteins was confirmed by ESI−MS (see Table 1).

Spectroscopic Analysis of the Protein Structure. Far-ultraviolet circular dichroism (UV CD) spectra were measured taking 10 scans from 260 to 190 nm in a J-810 spectropolarimeter (Jasco, U.K.). For determination of protein secondary and tertiary structures, the protein was dialyzed into 10 mM Na_2HPO_4 and 0.5 mM tris(2-carboxyethyl) phosphine (TCEP) (Fisher, U.K.) at pH 7 overnight at 4 °C containing either 50 μM Zn^{2+} ions or 1 mM ethylenediaminetetraacetic acid (EDTA). The comparison of spectra of RAR1 with varying metal occupancy was carried out in 25 mM ammonium acetate and 1 mM DTT at pH 4.0−6.5 after overnight dialysis at 4 °C. Near-UV CD spectra were measured taking 10 scans from 350 to 250 nm in a J-810 spectropolarimeter (Jasco, U.K.); the protein was dialyzed overnight in 20 mM *N*-2-hydroxyethylpiperazine-*N*′-2-ethanesulfonic acid (HEPES)-NaOH at pH 7.5 and 1 mM DTT with or without 1 mM EDTA. Fluorescence spectra were measured with a Fluoromax-3 spectrofluorimeter (Jobin Yvon, Edison, NJ) at 25 °C. Excitation wavelengths of 280 or 295 nm were used, with the averaged emission spectra of 5 (denaturation experiments) or 10 scans from 300 to 450 nm measured, using a bandwidth of 3 nm for excitation and emission slits. For thermal denaturation experiments, the cuvette was heated to the desired temperature (20−85 °C) and incubated for 5 min prior to taking measurements. For chemical denaturation with guanidine, the protein in 20 mM HEPES-NaOH and 1 mM DTT at pH 7.5 was mixed with 6.6 M guanidine in 20 mM HEPES-NaOH and 1 mM DTT at pH 7.5 to give 5 μM protein in 0−6 M final guanidine at 0.25 M intervals and incubated for 2 h at room temperature prior to measuring spectra. Denaturation by pH was carried out in 25 mM ammonium acetate at pH 3.5−8.0 after 2 h of incubation at room temperature. All spectra were run against a relevant buffer blank.

Proteolytic Stability of the Protein. Resistance to 0.01% trypsin (w/w) over a 3 h time course at 37 °C was carried out with 8 μM HvRAR1, predialyzed overnight at 4 °C into

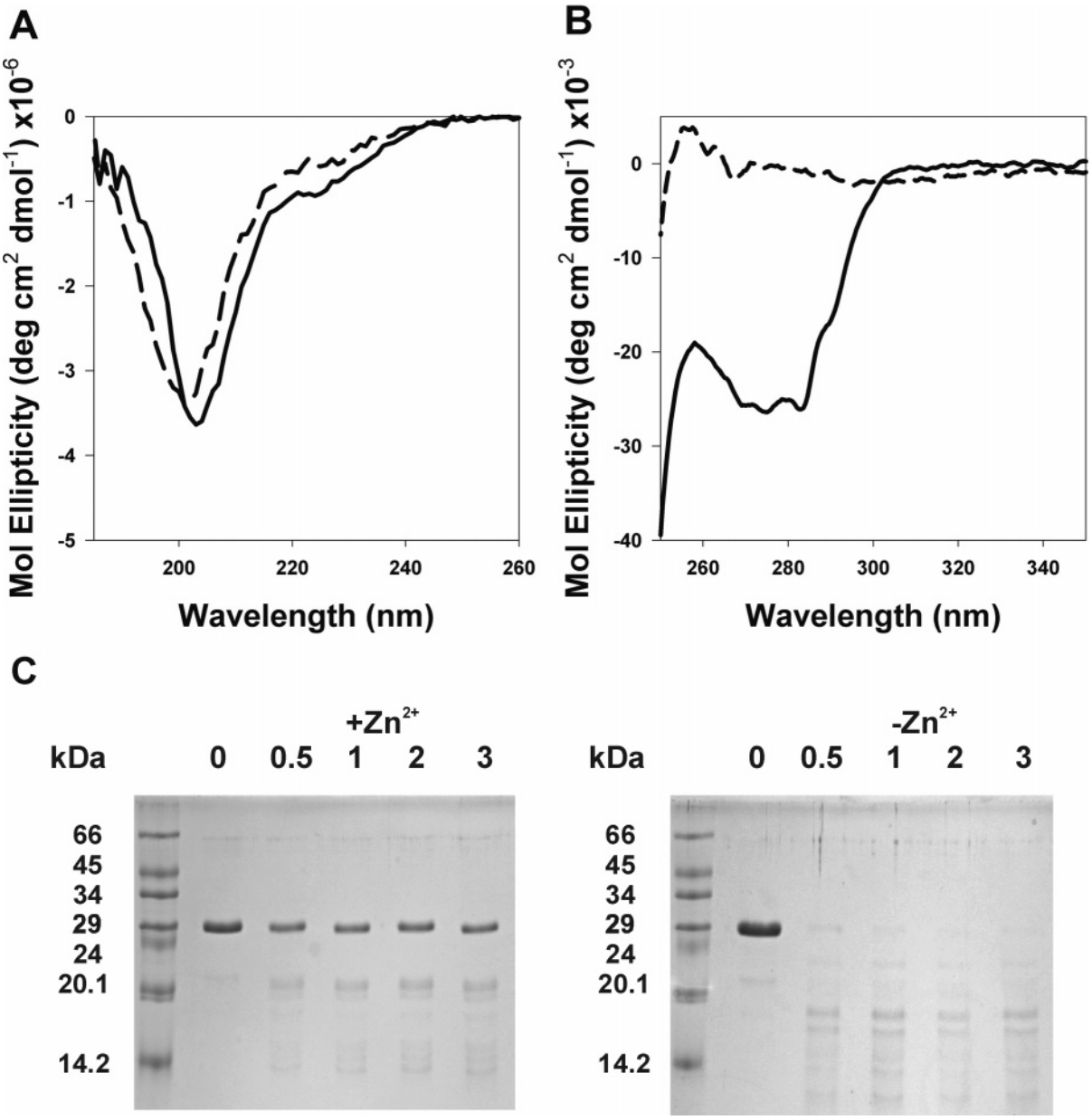

FIGURE 3: Removal of metal ions results in structural changes in AtRAR1. (A) Comparison of zinc-bound AtRAR1 (—, minimum of 205 nm) and EDTA-treated AtRAR1 (- - -, minimum of 197 nm) in 10 mM sodium phosphate at pH 7.5 by far-UV CD, showing that AtRAR1 has no discernible α-helical content. (B) Change in near-UV CD spectra of AtRAR1 in 20 mM HEPES-NaOH and 1 mM DTT at pH 7.5 with zinc-bound (—) or EDTA-treated (- - -) AtRAR1. (C) Trypsin treatment of HvRAR1 over a 0−3 h time course shows how zinc (left panel) protects the protein against proteolytic degradation relative to the apoprotein (right panel).

10 mM NaP_i and 0.5 mM TCEP at pH 7.5 with 50 μM zinc acetate or 1 mM EDTA. Reactions were stopped by boiling for 3 min in SDS−PAGE sample buffer containing 1.4 M β-mercaptoethanol, run on 16% SDS−PAGE gel (*36*), and visualized by Coomassie Blue staining.

Determination of the Protein Mass and Metal Content. Molecular masses were determined by electrospray ionization (ESI) using a Qstar tandem mass spectrometer (ABI Sciex, Foster City, CA), calibrated with cesium iodide and Bachem peptide H-9985. For masses determined using denaturing mass spectrometry (MS), proteins were diluted to 1 μM using 50% acetonitrile and 0.1% formic acid and infused via the ionspray source at a capillary voltage of 4700 V, with a flow rate between 9 and 3 μL min^{-1}. All constructs gave the expected mass determined from their peptide sequence within the specified 1:10 000 Da accuracy of the instrument (Table 1). Native-state MS for measuring bound metal was carried out in 25 mM ammonium acetate at pH 6.5−4.0. Proteins were dialyzed into 25 mM ammonium acetate at pH 7.5 and 1 mM DTT overnight at 4 °C prior to dilution in ammonium acetate buffer at the required pH, such that a 10 or 5 μM sample was sprayed at a flow rate of 10−7 μL min^{-1}. The capillary voltage was set at 4800 V. The analysis of bound metal was also determined using atomic absorption spectroscopy to identify and quantify the metal bound to RAR1. Protein samples were diluted to 5 μM, as determined by bovine serum albumin (Sigma, U.K.) calibration using the Bradford assay (BioRad, U.K.), in 0.5 mL buffer, made up to 1 mL with concentrated HCl, and incubated for 30 min at room temperature before making up to 5 mL with MilliQ double-deionized water at 18 MΩ and loading into a Ciros Vision (Spectro, Germany). Zinc concentrations were de-

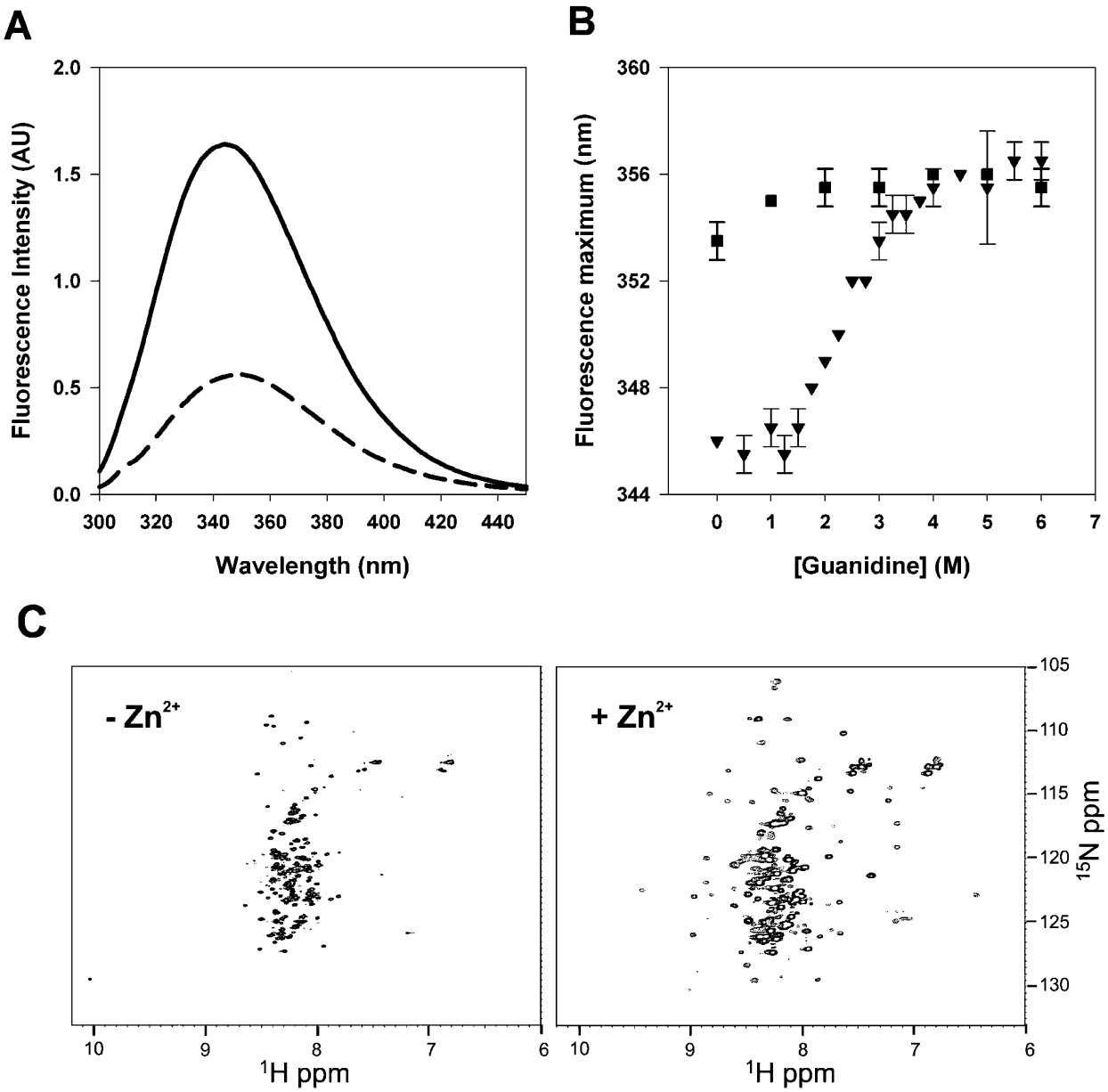

FIGURE 4: Folded structure of RAR1 is dependent upon the presence of zinc. AtRAR1 fluorescence spectra were measured in 20 mM HEPES-NaOH and 1 mM DTT at pH 7.5. (A) Fluorescence spectra of AtRAR1 with zinc-bound (—) and EDTA-treated (- - -) AtRAR1 show signal quenching and red shifting of λ_{max} from 345 to 354 nm. (B) Guanidine denaturation curves of AtRAR1 with zinc-bound (▼) or EDTA-treated (■) AtRAR1 determined by changes in tryptophan fluorescence λ_{max}. (C) $^{1}H-^{15}N$ HSQC spectra of HvCHORD-I in the absence (left panel) and presence (right panel) of zinc, showing the importance of metal ions for spectral dispersion and hence the structure of the domain.

termined against a standard curve of $Zn_{(aq)}$ (Sigma-Aldrich, U.K.) at 0, 5, 10, and 20 μM in 5 mL of MilliQ water.

NMR Spectroscopy. Spectra were measured on a VARIAN Unity plus spectrometer operating at 499.856 MHz for ^{1}H. Heteronuclear single-quantum coherence (HSQC) spectra were acquired using 1024 points in the ^{1}H dimension and 64 increments in the ^{15}N dimension with 8 transients. Samples were 0.5 mM HvCHORD-I in 20 mM Tris at pH 7.5, 100 mM NaCl, and 5 mM DTT.

Analytical Size-Exclusion Chromatography. The gel filtration was carried out using a Superdex 75 30/10 column (Amersham Pharmacia, U.K.) in 50 mM Tris-HCl at pH 7.5, 5 mM DTT, and 150 mM NaCl with either 50 μM $ZnCl_2$ for Zn^{2+} bound or 5 mM EDTA for metal free. Proteins were predialyzed into the appropriate buffer before loading onto the column, which had been calibrated using the LMW gel-filtration calibration kit (Amersham Biosciences, U.K.) in 50 mM Tris-HCl at pH 7.5, 150 mM NaCl, and 50 μM $ZnCl_2$.

Analytical Ultracentrifugation. Velocity and equilibrium sedimentation was carried out using a Beckman XL-I centrifuge with an AN60Ti rotor (Beckman, Fullerton, CA) at 10 °C. Protein sedimentation was followed by absorbance at 280 nm. All protein samples were measured against a buffer blank of 10 mM Na_2HPO_4 and 2.5 mM TCEP at pH 7.5. For sedimentation velocity runs, the protein was diluted to give an $A_{280} = 0.8$ (1.25 mg mL^{-1} AtRAR1) and samples were spun at 45 000 rpm, constantly scanning until plateau regions were lost in the scan. For equilibrium runs, proteins were diluted to $A_{280} = 0.4$ (0.62 mg mL^{-1} AtRAR1) and serially diluted 1:2 twice to give three concentrations for analysis at 16 000 and 23 000 rpm; readings were taken every

4 h until equilibrium was reached. Data were analyzed using SEDFIT (*37*) software with densities and viscosities estimated by SEDNTERP (*38*).

Isothermal Titration Calorimetry (ITC). ITC measurements were performed using a MicroCal VP-ITC thermostated at 25 °C. HvSGT1 and AtCHORD-II were extensively dialyzed against 50 mM Tris-HCl and 1 mM TCEP at pH 7.5. HvSGT1 at 38.5 μM was loaded into the cell, and AtCHORD-II at 565.8 μM was loaded into the syringe. Heats of binding at 25 °C were measured from 30 injections of 10 μL each. For EDTA-treated AtCHORD-II, both HvSGT1 and AtCHORD-II were extensively dialyzed into 50 mM Tris-HCl and 1 mM TCEP at pH 7.5 with initially 5 mM EDTA and then 1 mM EDTA. HvSGT1 in the syringe at 640.7 μM was injected into 37.7 μM AtCHORD-II, and the heat of binding at 20 °C was measured. The heats of dilution (AtCHORD-II against buffer) were subtracted from the binding data, and binding parameters were determined using Origin software.

RESULTS AND DISCUSSION

Expression and Purification of Barley and Arabidopsis RAR1 and Their Derivatives. In this study, we have used intact and domain constructs of barley (Hv) and *Arabidopsis* (At) RAR1 (Figure 1), with hexa-His or GST purification tags. Using two homologues of RAR1 purified by different strategies has allowed for a comparison of their physical properties from which a consensus could be reached about native RAR1. Proteins were purified using Zn^{2+}-NTA- or glutathione-affinity chromatography for His- or GST-tagged proteins, respectively. The tags were then removed using TEV or PreScission proteases as described in the Experimental Procedures. Aggregates and impurities were removed subsequently by size-exclusion and ion-exchange chromatography. AtRAR1, AtCHORD-I-CCCH, AtCHORD-II, HvRAR1, HvCHORD-I, and HvCHORD-II were visualized on reducing 16% SDS−PAGE and shown to be >95% pure (Figure 2). The mass of each protein was confirmed by denaturing ESI−MS, with observed masses within 1−2 Da of the calculated values (Table 1).

Role of Zinc in Maintaining RAR1 and CHORD Stability. Previous work showed that RAR1 is a zinc metalloprotein, containing two zinc-binding CHORDs believed to have a novel fold (*4*). Using the two plant RAR1 homologues purified in zinc-containing buffers, we investigated the structure of intact RAR1. Secondary-structure determination using far-UV CD spectra of metal-bound AtRAR1 showed little apparent α-helical content because no significant minimum at ~220 nm was seen (Figure 3A). Both barley and *Arabidopsis* RAR1 gave very similar spectra, with a single minimum at 205 nm, suggesting that the spectra are common to both homologues and represent the native RAR1 structure (Figure 3A and data not shown). Deconvolution of the spectra using CDNN software (Martin-Luther-University, Halle-Wittenberg, Germany) suggested little apparent structure in these purified proteins, however, with their spectra more similar to those of unfolded polypeptides (which generally have a minimum ~ 197 nm). An alternative explanation is that RAR1 is rich in β structure because these often display far-UV CD spectra with single minima close to 200 nm [for example, soybean trypsin inhibitor and elastase (*39*)]. This led us to investigate whether our purified

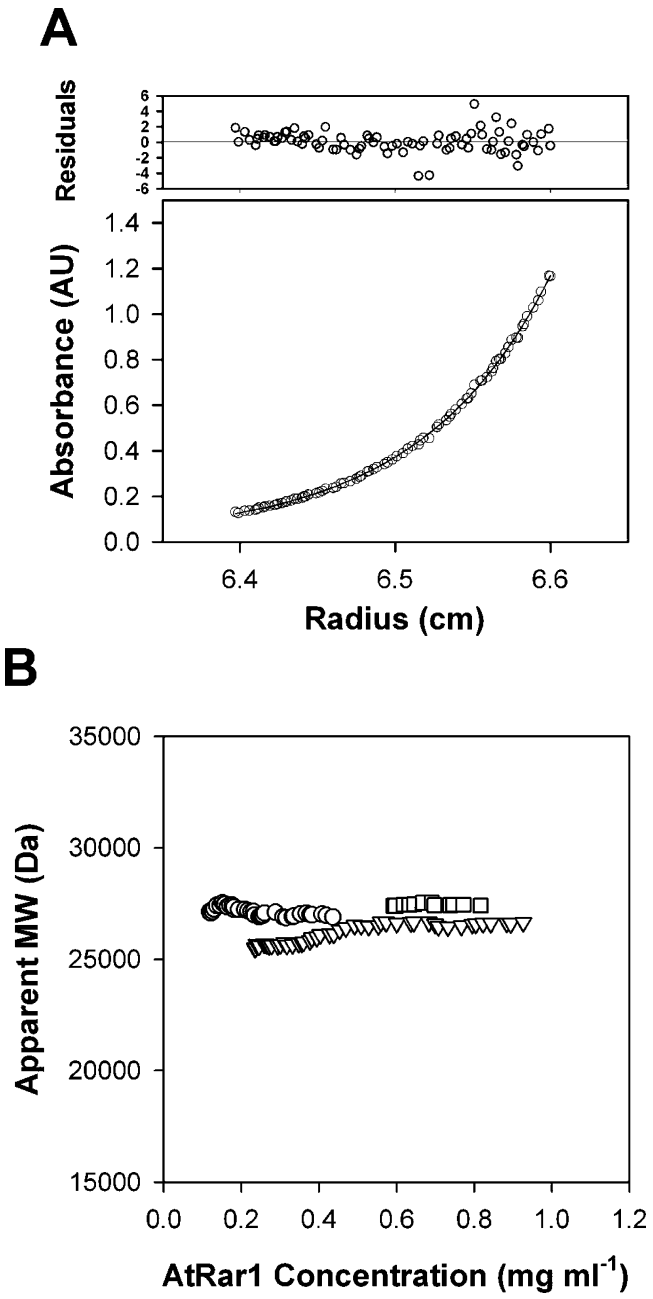

FIGURE 5: AtRAR1 is a monomer in solution as determined by equilibrium sedimentation. AtRAR1 in 20 mM Tris-HCl at pH 7.5 and 2 mM TCEP was centrifuged at 23 000 rpm. (A) Experimental data (○) plotted with a theoretical single fit for a 26 kDa species (—) with residuals shown above, $C(r) = C(r_0)\exp[(w^2/2RT)M(1 - \upsilon_{bar}\rho)(r^2 - r_0^2)]$. (B) Plot of the apparent molecular weight against the concentration from three runs shows RAR1 to be monomeric in solution with an apparent mass of ~26 kDa.

RAR1 preparations from barley and *Arabidopsis* were unfolded.

To assess whether RAR1 was folded, we measured the far-UV CD spectrum of EDTA-treated protein to investigate if there are structural changes on chelation of bound metal. The removal of metal led to a decrease in the minimum from 205 to 197 nm for both AtRAR1 and HvRAR1 (Figure 3A, data not shown). To ascertain whether this change was due to secondary-structure rearrangement or unfolding, the tertiary structure of AtRAR1 was probed using near-UV CD (Figure 3B). The loss of signal from the 3 tryptophan and 15 phenylalanine residues of AtRAR1 between the metal-

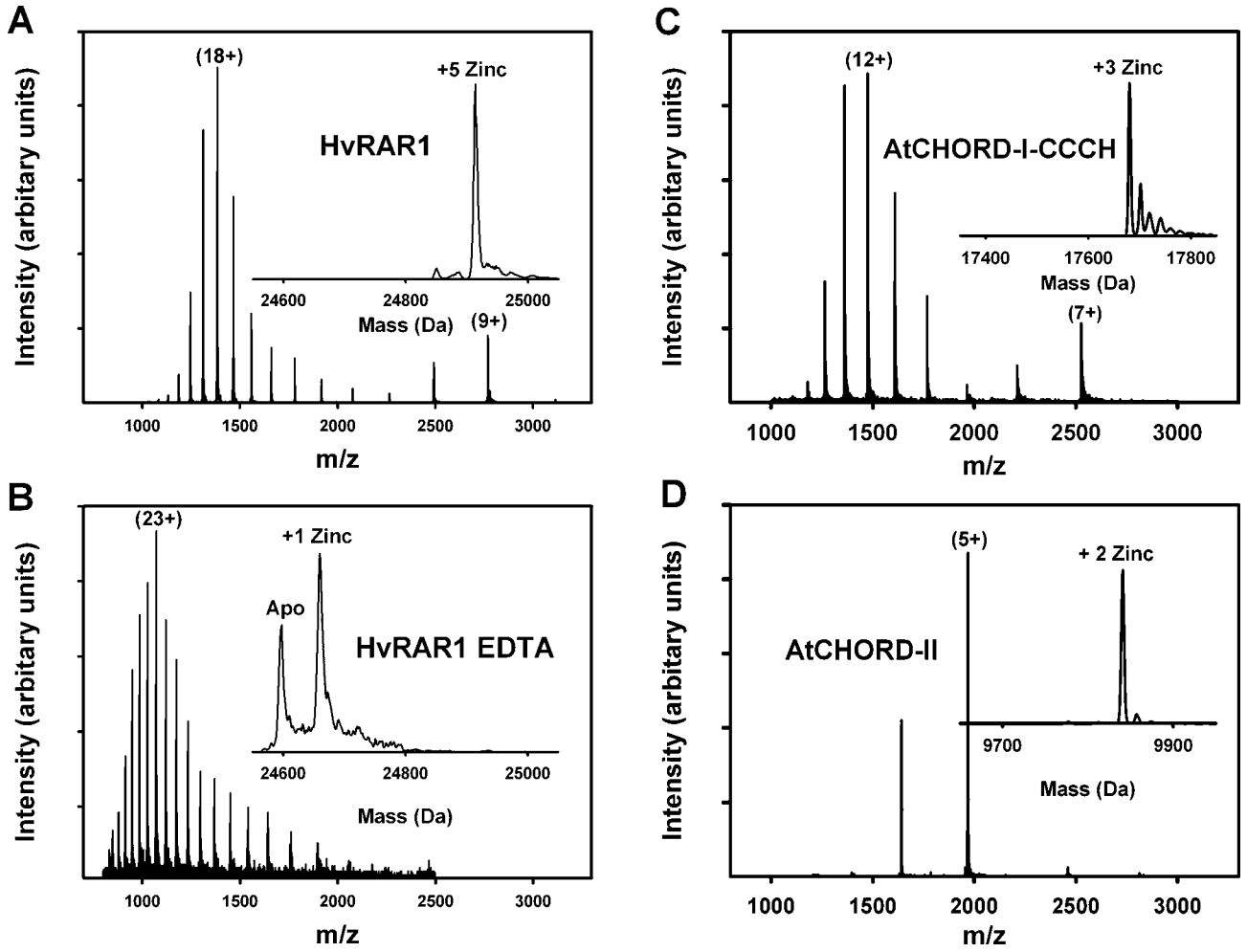

FIGURE 6: RAR1 and CHORD zinc stoichiometry determined by native-state ESI−MS. The protein was injected into a Qstar mass spectrometer (ABI Sciex, Foster City, CA) in 25 mM ammonium acetate at pH 6.5. Plots of *m*/*z* against the intensity show main charge species in parenthesis for each distribution. Inserts are plots of reconstructed masses against the intensity of species present. (A) HvRAR1, peak at 24 915 Da; (B) HvRAR1 with prior EDTA treatment, peaks at 24 599 and 24 662 Da; (C) AtCHORD-I-CCCH, peak at 17 679 Da; and (D) AtCHORD-II, peak at 9840 Da. RAR1 binds five Zn^{2+} ions, with each CHORD binding two Zn^{2+} ions and the CCCH motif binding one. EDTA treatment of all proteins leads to the loss of bound zinc. All protein masses ± zinc are presented in Table 1.

bound and EDTA-treated material shows that the aromatic residues in the zinc-depleted samples experience an increase in side-chain mobility, suggesting that AtRAR1 unfolds upon the loss of zinc. Tryptic digests of RAR1 in the presence and absence of metal further supported the findings that RAR1 is destabilized in the absence of metal because zinc confers resistance to proteolytic degradation (Figure 3C).

Additional evidence that our purified RAR1 preparations were folded came from intrinsic tryptophan fluorescence spectroscopy (Figure 4A). Excitation at 295 nm of *Arabidopsis* RAR1 (and barley, data not shown) confirmed that the metal-bound form is folded. AtRAR1 shows a fluorescence maximum of 344 nm, which red-shifts (and quenches) to 356 nm upon treatment with EDTA, consistent with the environment of the aromatic residues changing from nonpolar to polar when bound metal is removed. The role of zinc was further investigated by chemical denaturation using tryptophan fluorescence. Metal-bound or EDTA-treated AtRAR1 were mixed with increasing concentrations of guanidine hydrochloride (Figure 4B). Zinc-bound RAR1 exhibits a complex unfolding behavior consistent with a multidomain protein, with half-maximal unfolding at 2.39 ± 0.07 M guanidine-HCl. In contrast, metal-free protein showed little change in λ_{max} with an increasing denaturant, consistent with the protein being already unfolded. Analysis of the zinc-bound AtRAR1 constructs, AtCHORD-I-CCCH and AtCHORD-II, gave values for half-maximal unfolding of 1.74 ± 0.02 and 2.20 ± 0.03 M guanidine-HCl, respectively (data not shown). Zinc-bound HvCHORD-I and HvCHORD-II were found to be slightly more resistant to unfolding at 2.53 ± 0.08 and 2.91 ± 0.05 M guanidine, respectively (data not shown). Each expressed CHORD, just like full-length RAR1, exhibited zinc dependence for guanidine-induced denaturation and appeared unfolded upon the removal of metal. The fact that the removal of the metal ion unfolds these domains was reinforced by heteronuclear NMR experiments on ^{15}N-labeled HvCHORD-I and $^{1}H-^{15}N$ HSQC spectra, which are exquisitely sensitive to protein fold (*40*). The collapse of the amide HSQC peaks of the zinc-free protein indicates the unfolding of the CHORD-I (Figure 4C), supporting the previous spectroscopic data that implicate zinc as essential for maintaining the RAR1 structure. It is interesting to note that the presence of amide peaks in the region of 8.8−10 ppm is suggestive of CHORD containing at least some β-sheet structure.

The half-maximal guanidine-HCl denaturation of the full-length AtRAR1 was similar to that of the isolated domains AtCHORD-I-CCCH and AtCHORD-II, suggesting that there

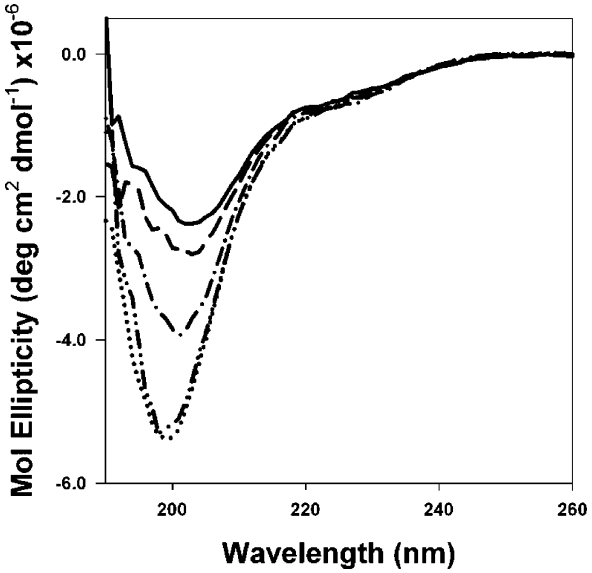

FIGURE 7: Progressive removal of zinc ions induces the loss of HvRAR1 secondary structure. Far-UV CD spectra of HvRAR1 in 25 mM ammonium acetate with a decreasing pH shows the minimum decreasing from 203 nm at pH 6.5 to 199 nm below pH 4.0 with a concurrent increase in negative ellipticity. ESI−MS spectra were taken at each pH (6.5, 5.5, 5, 4, and 3.1) that showed a diminution of bound metal ion: predominantly five at the higher pH values (6.5 and 5.5), a variable number at pH 5, and no bound zinc at low pH values (4 and 3.1).

may be little interaction between the two CHORDs within RAR1. A comparison of AtRAR1 and AtCHORD-II by thermal denaturation also gave similar T_m values: 62 °C for AtRAR1 and 56 °C for AtCHORD-II. Similarly, unfolding for zinc-bound protein using decreasing pH gave half-maximal unfolding at pH 5.35 for AtRAR1, pH 5.28 ± 0.01 for AtCHORD-I-CCCH, and pH 5.58 ± 0.02 for AtCHORD-II. These findings suggest the CHORDs act as autonomous units having few intramolecular connections. In summary, the spectroscopic analysis of AtRAR1 and HvRAR1 has revealed that they have similar properties; the proteins and their component CHORDs are folded, nonhelical proteins that are dependent upon zinc for structural integrity.

Analytical Ultracentrifugation Analysis of RAR1. RAR1 elutes from gel-filtration columns with an apparent molecular weight of 50 kDa (data not shown), suggesting that the protein is either a dimer or a monomer that elutes anomalously. Sedimentation equilibrium runs of AtRAR1 showed the protein to have a concentration-independent average molecular weight of ~26 kDa (Figure 5), while sedimentation velocity experiments yielded a sedimentation coefficient of 1.6 S at 10 °C ($S_{20,w}$ = 2.20 S) and a frictional ratio (f/f_0) of 1.69 ± 0.06. When these data are taken together, they show that RAR1 is a monomer with an extended, nonspherical conformation, consistent with the lack of interdomain interactions implied from the earlier denaturation data.

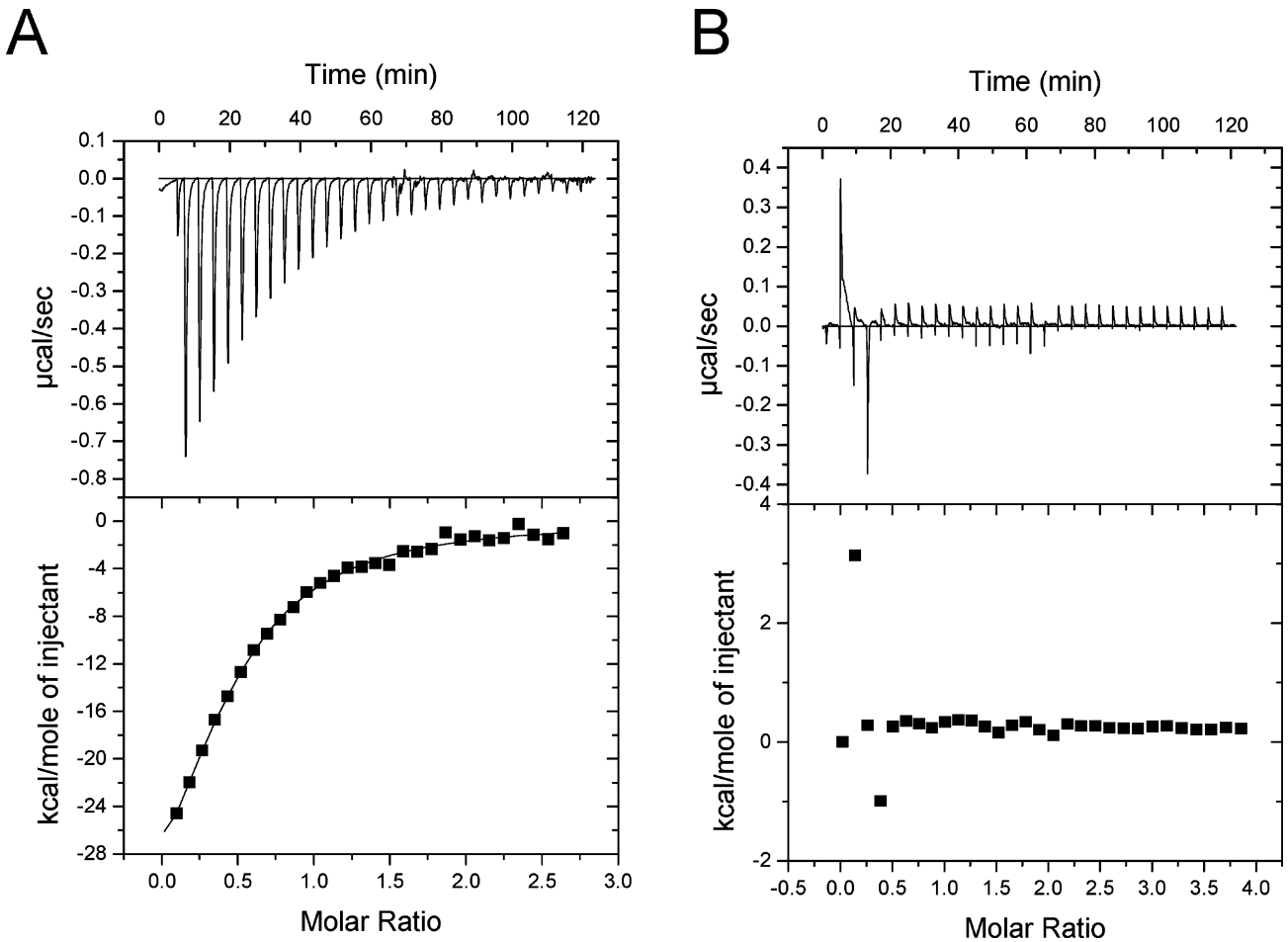

FIGURE 8: CHORD-II interaction with SGT1 is zinc-dependent and weak. (A) ITC isotherm for HvSGT1 binding zinc-loaded AtCHORD-II. Data, which were fitted to a single-binding-site model, indicate that binding is weak. The equilibrium dissociation constant (K_d) was determined to be 6.7 ± 0.4 μM (stoichiometry n = 1.1 ± 0.3) from two independent measurements in 50 mM Tris containing 1 mM TCEP at pH 7.5. (B) ITC isotherm for HvSGT1 binding to zinc-depeleted AtCHORD-II shows no interaction occurs upon mixing.

RAR1 and CHORD Zinc-Binding Analysis. Sequence analysis of RAR1 shows it to have five potential metal-binding sites. Four of these sites are located within the two CHORDs and are all conserved residues, with the fifth potential site in the plant-specific CCCH motif (Figure 1). Initial metal analysis reported RAR1 to bind two zinc ions, one in each CHORD (*4*). As we have shown zinc to play a significant role in maintaining the structure of RAR1 and its CHORDs, we reinvestigated the metal stoichiometry to see whether the structural integrity of each CHORD was dependent upon a single zinc ion. To determine the metal content of RAR1 and the individual CHORDs, ESI−MS and atomic absorption spectroscopy were used. ESI−MS was used as a qualitative method to determine the mass of the proteins under native (metal-bound) and denaturing (metal-free) conditions, whereas atomic absorption spectroscopy was used to quantitatively determine the metal content. Under native conditions, RAR1 proteins from both barley (Figure 6A) and *Arabidopsis* were 316.7 Da heavier than their denatured states (Table 1), an increase in the mass equivalent to five Zn^{2+} ions: $(65.4 - 2H^+)5 = 317$. Furthermore, the individual CHORDs shared a difference in mass of between 127.2 and 127.9 Da, equivalent to two Zn^{2+} ions: $(65.4 - 2H^+)2 = 126.8$ (Figure 6C). The CHORD-I-CCCH truncate under native conditions had a mass increase of 191.1 Da, equivalent to three Zn^{2+} ions: $(65.4 - 2H^+)3 = 190.2$ (Figure 6D). Atomic absorption spectroscopy confirmed the identity of the metal ion as zinc and corroborated the stoichiometries for all of the *Arabidopsis* constructs and barley RAR1 (Table 1). If the ligand is noncovalently bound zinc, then the treatment of RAR1 with EDTA prior to running native-state ESI−MS should just yield the calculated mass of RAR1. A comparison of parts A and B of Figure 6 shows that the mass for the apo form of RAR1 was obtained by the addition of EDTA, indicating that zinc is specifically co-ordinated to RAR1. Treatment with EDTA usually gave both apoprotein and protein bound to one zinc ion as seen in Figure 6B. Our analysis of the individual CHORDs from barley and *Arabidopsis* show that each CHORD binds two zinc ions. The remaining zinc binds to the CCCH motif, establishing for the first time a zinc-binding role for the motif.

We next investigated whether the change in structure observed by far-UV CD that results from a decreasing pH (see above) could correspond to the sequential loss of zinc (Figure 7). We found using ESI−MS that as the pH was reduced the number of zinc ions co-ordinated by RAR1 reduced from five at pH 6.5 to none at pH 4.0 (data not shown). Moreover, at intermediate pH values, a mixture of species were seen corresponding to four-, three-, two-, and one-bound zinc. Thus, there is a correlation between the extent of protein unfolding by pH and the number of metal ions lost from the protein, confirming that the interaction between zinc and RAR1 is specific and functional with respect to the protein structure. We conclude that RAR1 is a zinc−metalloprotein able to coordinate five zinc ions and not two as previously described. Moreover, these metal ions are essential for stabilizing and maintaining the folded conformation of the intact protein and its CHORDs.

Metal-Dependent Binding Interaction. RAR1 has been shown to interact with SGT1 through CHORD-II and HSP90 through CHORD-I by yeast two-hybrid analysis and immunoprecipitation (*13*). The majority of the previously reported interactions has relied on cell extracts or *in vitro* transcription and translation (*12*, *13*). In the present study, we used ITC to define more precisely the conditions for the interaction between AtRAR1 and barley SGT1 (HvSGT1). Binding between zinc-bound and EDTA-treated AtCHORD-II (no bound metal) with HvSGT1 was invesigated (Figure 8). Only zinc-bound AtCHORD-II was able to bind HvSGT1, which was stoichiometric and weak ($K_d \sim 7$ μM), with near identical data obtained for intact RAR1 (data not shown). This interaction is weaker by an order of magnitude than the protein−protein interaction mediated by the zinc-binding RING domain of the corepressor KAP-1, when binding the KRAB transcription repression domain of KOX-1, $K_d = 142$ nM (*41*). This result also confirms that the interaction between RAR1 and SGT1 is through CHORD-II and that the association is conserved between monocotyledonous and dicotyledonous plants, as previously reported (*13*). Whether binding between barley CHORD-II and barley SGT1 would result in a stronger interaction is unclear, because *in vivo* interactions have been readily detectible between barley RAR1 and *Arabidopsis* SGT1, *Arabidopsis* RAR1 and barley SGT1, and even barley HSP90 and *Arabidopsis* RAR1 or SGT1 (*5*, *13*).

CONCLUSIONS

Characterization of RAR1 and its CHORDs, with respect to their structural stability and interactions with the binding partner SGT1, has led to the identification of zinc playing an important role. The biophysical analysis of RAR1 shows that the maintenance of both the secondary and tertiary structure is strictly dependent upon the presence of bound zinc ions. CHORDs require two zinc ions to stabilize their structure for mediating protein−protein interactions, because the loss of zinc from RAR1 or CHORD-II prevented SGT1 binding. Furthermore, the CCCH motif linking the CHORDs of RAR1 also binds zinc, furnishing RAR1 with five zinc-binding sites, rather than two as first reported (*4*). The sensitivity of RAR1 to pH denaturation with half-maximal denaturation at pH 5.35 suggests that at least one of the zinc ligands, in one or more of the metal-binding sites, is likely to be a histidine residue, consistent with the two conserved Cys_3His motifs in each CHORD. RAR1 adopts an elongated conformation with little or no interaction between each separate CHORD. The intervening zinc-binding plant-specific CCCH motif may simply be a bridge or spacer between the two functional CHORDs of RAR1. The absence of any significant helical structure in the CHORD suggests that this module does not belong to classical $\beta\beta\alpha$ or RING domain classes of zinc-finger proteins (*42*−*45*).

ACKNOWLEDGMENT

We are indebted to Afua Nyarko (York) for the ITC data presented in this paper, Ewald van den Bremer (Utrecht) for preliminary ESI−MS metal analysis, Berni Strongitharm (York) for technical assistance with ESI−MS experiments, and Adam Cartwright (York) for undertaking the initial metal analysis of AtCHORD-II. We also thank Dan Walker and Afua Nyarko for critical reading of the manuscript.

REFERENCES

1. Shirasu, K., and Schulze-Lefert, P. (2000) Regulators of cell death in disease resistance, *Plant Mol. Biol. 44*, 371−385.

2. Heath, M. C. (2000) Hypersensitive response-related death, *Plant Mol. Biol. 44*, 321−334.
3. Freialdenhoven, A., Scherag, B., Hollricher, K., Collinge, D. B., Thordal-Christensen, H., and Schulze-Lefert, P. (1994) Nar-1 and Nar-2, two loci required for Mla12-specified race-specific resistance to powdery mildew in barley, *Plant Cell 6*, 983−994.
4. Shirasu, K., Lahaye, T., Tan, M. W., Zhou, F., Azevedo, C., and Schulze-Lefert, P. (1999) A novel class of eukaryotic zinc-binding proteins is required for disease resistance signaling in barley and development in *C. elegans*, *Cell 99*, 355−366.
5. Takahashi, A., Casais, C., Ichimura, K., and Shirasu, K. (2003) HSP90 interacts with RAR1 and SGT1 and is essential for RPS2-mediated disease resistance in *Arabidopsis*, *Proc. Natl. Acad. Sci. U.S.A. 100*, 11777−11782.
6. Muskett, P. R., Kahn, K., Austin, M. J., Moisan, L. J., Sadanandom, A., Shirasu, K., Jones, J. D. G., and Parker, J. E. (2002) *Arabidopsis* RAR1 exerts rate-limiting control of R gene-mediated defenses against multiple pathogens, *Plant Cell 14*, 979−992.
7. Tornero, P., Merritt, P., Sadanandom, A., Shirasu, K., Innes, R. W., and Dangl, J. L. (2002) RAR1 and NDR1 contribute quantitatively to disease resistance in *Arabidopsis*, and their relative contributions are dependent on the R gene assayed, *Plant Cell 14*, 1005−1015.
8. Baraldi, E., Carugo, K. D., Hyvonen, M., Surdo, P. L., Riley, A. M., Potter, B. V., O'Brien, R., Ladbury, J. E., and Saraste, M. (1999) Structure of the PH domain from Bruton's tyrosine kinase in complex with inositol 1,3,4,5-tetrakisphosphate, *Structure 7*, 449−460.
9. Brancaccio, M., Fratta, L., Notte, A., Hirsch, E., Poulet, R., Guazzone, S., De Acetis, M., Vecchione, C., Marino, G., Altruda, F., Silengo, L., Tarone, G., and Lembo, G. (2003) Melusin, a muscle-specific integrin β_1-interacting protein, is required to prevent cardiac failure in response to chronic pressure overload, *Nat. Med. 9*, 68−75.
10. Sadanandom, A., Findlay, K., Doonan, J. H., Schulze-Lefert, P., and Shirasu, K. (2004) CHPA, a cysteine- and histidine-rich-domain-containing protein, contributes to maintenance of the diploid state in *Aspergillus nidulans*, *Eukaryotic Cell 3*, 984−991.
11. Hahn, J. S. (2005) Regulation of Nod1 by Hsp90 chaperone complex, *FEBS Lett. 579*, 4513−4519.
12. Hubert, D. A., Tornero, P., Belkhadir, Y., Krishna, P., Takahashi, A., Shirasu, K., and Dangl, J. L. (2003) Cytosolic HSP90 associates with and modulates the *Arabidopsis* RPM1 disease resistance protein, *EMBO J. 22*, 5679−5689.
13. Azevedo, C., Sadanandom, A., Kitagawa, K., Freialdenhoven, A., Shirasu, K., and Schulze-Lefert, P. (2002) The RAR1 interactor SGT1, an essential component of R gene-triggered disease resistance, *Science 295*, 2073−2076.
14. Rutherford, S. L., and Lindquist, S. (1998) Hsp90 as a capacitor for morphological evolution, *Nature 396*, 336−342.
15. Kosano, H., Stensgard, B., Charlesworth, M. C., McMahon, N., and Toft, D. (1998) The assembly of progesterone receptor−hsp90 complexes using purified proteins, *J. Biol. Chem. 273*, 32973−32979.
16. Sangster, T. A., and Queitsch, C. (2005) The HSP90 chaperone complex, an emerging force in plant development and phenotypic plasticity, *Curr. Opin. Plant Biol. 8*, 86−92.
17. Caplan, A. J. (1999) Hsp90's secrets unfold: New insights from structural and functional studies, *Trends Cell Biol. 9*, 262−268.
18. Meyer, P., Prodromou, C., Hu, B., Vaughan, C., Roe, S. M., Panaretou, B., Piper, P. W., and Pearl, L. H. (2003) Structural and functional analysis of the middle segment of Hsp90: Implications for ATP hydrolysis and client protein and cochaperone interactions, *Mol. Cell 11*, 647−658.
19. Panaretou, B., Prodromou, C., Roe, S. M., O'Brien, R., Ladbury, J. E., Piper, P. W., and Pearl, L. H. (1998) ATP binding and hydrolysis are essential to the function of the Hsp90 molecular chaperone in vivo, *EMBO J. 17*, 4829−4836.
20. Pearl, L. H., and Prodromou, C. (2000) Structure and in vivo function of Hsp90, *Curr. Opin. Struct. Biol. 10*, 46−51.
21. Kitagawa, K., Skowyra, D., Elledge, S. J., Harper, J. W., and Hieter, P. (1999) SGT1 encodes an essential component of the yeast kinetochore assembly pathway and a novel subunit of the SCF ubiquitin ligase complex, *Mol. Cell 4*, 21−33.
22. Austin, M. J., Muskett, P., Kahn, K., Feys, B. J., Jones, J. D. G., and Parker, J. E. (2002) Regulatory role of SGT1 in early R gene-mediated plant defenses, *Science 295*, 2077−2080.
23. Liu, Y., Schiff, M., Serino, G., Deng, X. W., and Dinesh-Kumar, S. P. (2002) Role of SCF ubiquitin-ligase and the COP9 signalosome in the N gene-mediated resistance response to tobacco mosaic virus, *Plant Cell 14*, 1483−1496.
24. Peart, J. R., Lu, R., Sadanandom, A., Malcuit, I., Moffett, P., Brice, D. C., Schauser, L., Jaggard, D. A., Xiao, S., Coleman, M. J., Dow, M., Jones, J. D., Shirasu, K., and Baulcombe, D. C. (2002) Ubiquitin ligase-associated protein SGT1 is required for host and nonhost disease resistance in plants, *Proc. Natl. Acad. Sci. U.S.A. 99*, 10865−10869.
25. Dubacq, C., Guerois, R., Courbeyrette, R., Kitagawa, K., and Mann, C. (2002) Sgt1p contributes to cyclic AMP pathway activity and physically interacts with the adenylyl cyclase Cyr1p/Cdc35p in budding yeast, *Eukaryotic Cell 1*, 568−582.
26. Lee, Y. T., Jacob, J., Michowski, W., Nowotny, M., Kuznicki, J., and Chazin, W. J. (2004) Human Sgt1 binds HSP90 through the CHORD-Sgt1 domain and not the tetratricopeptide repeat domain, *J. Biol. Chem. 279*, 16511−16517.
27. Garcia-Ranea, J. A., Mirey, G., Camonis, J., and Valencia, A. (2002) p23 and HSP20/α-crystallin proteins define a conserved sequence domain present in other eukaryotic protein families, *FEBS Lett. 529*, 162−167.
28. Russell, L. C., Whitt, S. R., Chen, M. S., and Chinkers, M. (1999) Identification of conserved residues required for the binding of a tetratricopeptide repeat domain to heat shock protein 90, *J. Biol. Chem. 274*, 20060−20063.
29. Das, A. K., Cohen, P. T. W., and Barford, D. (1998) The structure of the tetratricopeptide repeats of protein phosphatase 5: Implications for TPR-mediated protein−protein interactions, *EMBO J. 17*, 1192−1199.
30. Schadick, K., Fourcade, H. M., Boumenot, P., Seitz, J. J., Morrell, J. L., Chang, L., Gould, K. L., Partridge, J. F., Allshire, R. C., Kitagawa, K., Hieter, P., and Hoffman, C. S. (2002) *Schizosaccharomyces pombe* Git7p, a member of the *Saccharomyces cerevisiae* Sgtlp family, is required for glucose and cyclic AMP signaling, cell wall integrity, and septation, *Eukaryotic Cell 1*, 558−567.
31. Shen, Q. H., Zhou, F., Bieri, S., Haizel, T., Shirasu, K., and Schulze-Lefert, P. (2003) Recognition specificity and RAR1/SGT1 dependence in barley Mla disease resistance genes to the powdery mildew fungus, *Plant Cell 15*, 732−744.
32. Leister, R. T., Dahlbeck, D., Day, B., Li, Y., Chesnokova, O., and Staskawicz, B. J. (2005) Molecular genetic evidence for the role of SGT1 in the intramolecular complementation of Bs2 protein activity in *Nicotiana benthamiana*, *Plant Cell 17*, 1268−1278.
33. Holt, B. F., III, Belkhadir, Y., and Dangl, J. L. (2005) Antagonistic control of disease resistance protein stability in the plant immune system, *Science 309*, 929−932.
34. Azevedo, C., Betsuyaku, S., Peart, J. R., Takahashi, A., Noel, L., Sadanandom, A., Casais, C., Parker, J., and Shirasu, K. (2006) Role of SGT1 in resistance protein accumulation in plant immunity, *EMBO J. 25*, 2007−2016.
35. Scofield, S. R., Huang, L., Brandt, A. S., and Gill, B. S. (2005) Development of a virus-induced gene-silencing system for hexaploid wheat and its use in functional analysis of the Lr21-mediated leaf rust resistance pathway, *Plant Physiol.* 105.
36. Laemmli, U. K. (1970) Cleavage of structural proteins during the assembly of the head of bacteriophage T4, *Nature 227*, 680−685.
37. Laue, T. M., Shah, B. D., Ridgeway, T. M., and Pelletier, S. L. (1992) Computer-aided interpretation of analytical sedimenation data for proteins, *Anal. Ultracentrifugation Biochem. Polym. Sci.* 90−125.
38. Schuck, P. (2000) Size-distribution analysis of macromolecules by sedimentation velocity ultracentrifugation and lamm equation modeling, *Biophys. J. 78*, 1606−1619.
39. Wallace, B. A., Wien, F., Miles, A. J., Lees, J. G., Hoffmann, S. V., Evans, P., Wistow, G. J., and Slingsby, C. (2004) Biomedical applications of synchrotron radiation circular dichroism spectroscopy: Identification of mutant proteins associated with disease and development of a reference database for fold motifs, *Faraday Discuss. 126*, 237−243.
40. Dyson, H. J., and Wright, P. E. (2004) Unfolded proteins and protein folding studied by NMR, *Chem. Rev. 104*, 3607−3622.
41. Peng, H., Begg, G. E., Harper, S. L., Friedman, J. R., Speicher, D. W., and Rauscher, F. J., III (2000) Biochemical analysis of the Kruppel-associated box (KRAB) transcriptional repression domain, *J. Biol. Chem. 275*, 18000−18010.

42. Capili, A. D., Edghill, E. L., Wu, K., and Borden, K. L. B. (2004) Structure of the C-terminal RING finger from a RING-IBR-RING/TRIAD motif reveals a novel zinc-binding domain distinct from a RING, *J. Mol. Biol. 340*, 1117−1129.
43. McCarty, A. S., Kleiger, G., Eisenberg, D., and Smale, S. T. (2003) Selective dimerization of a C_2H_2 zinc finger subfamily, *Mol. Cell 11*, 459−470.
44. Saurin, A. J., Borden, K. L. B., Boddy, M. N., and Freemont, P. S. (1996) Does this have a familiar RING? *Trends Biochem. Sci. 21*, 208−214.
45. Bardwell, V. J., and Treisman, R. (1994) The POZ domain: A conserved protein−protein interaction motif, *Genes Dev. 8*, 1664−1677.
46. Lei, Q. P., Cui, X., Kurtz, D. M., Amster, I. J., Chernushevich, I. V., and Standing, K. G. (1998) Electrospray mass spectrometry studies of non-heme iron-containing proteins, *Anal. Chem. 70*, 1838−1846.

BI062174K